COMPOSITE POLYMER-COATED MINERAL SCAFFOLDS FOR BONE REGENERATION: FROM MATERIAL CHARACTERIZATION TO HUMAN STUDIES

G. PERTICI[1], F. CARINCI[2], G. CARUSI[3], D. EPISTATUS[4], T. VILLA[5,6], F. CRIVELLI[7], F. ROSSI[8] and G. PERALE[1,9]

[1]Industrie Biomediche Insubri SA, Mezzovico-Vira, Switzerland; [2]Department of Morphology, Surgery and Experimental Medicine, University of Ferrara, Ferrara, Italy [3]Private practice, Ponsacco, Italy; [4]Universitatea de Medicina si Farmacie "Carol Davila", Bucharest, Romania; [5]Politecnico di Milano, Laboratory of Biological Structure Mechanics, Department of Chemistry, Materials and Chemical Engineering "G. Natta", Milan, Italy; [6]IRCCS Istituto Ortopedico Galeazzi, Milan, ltaly; [7]Azienda Ospedaliera di Circolo, Busto Arsizio, Italy; [8]Politecnico di Milano, Physical Chemistry Laboratory, Department of Chemistry, Materials and Chemical Engineering "G. Natta", Milan, Italy; [9]Department of innovative Technologies, University for Applied Science and Art of Southern Switzerland, Manno, Switzerland

Bovine bone xenografts, made of hydroxyapatite (HA), were coated with poly(L-lactide-co-ε-caprolactone) (PLCL) and RGD-containing collagen fragments in order to increase mechanical properties, hydrophilicity, cell adhesion and osteogenicity. *In vitro* the scaffold microstructure was investigated with Environmental Scanning Electronic Microscopy (ESEM) analysis and micro tomography, while mechanical properties were investigated by means compression tests. In addition, cell attachment and growth within the three-dimensional scaffold inner structure were validated using human osteosarcoma cell lines (SAOS-2 and MG-63). Standard ISO *in vivo* biocompatibility studies were carried out on model animals, while bone regenerations in humans were performed to assess the efficacy of the product. All results from *in vitro* to *in vivo* investigations are here reported, underlining that this scaffold promotes bone regeneration and has good clinical outcome.

Evidence of clinical needs related to bone reconstruction dates back to ancient Egypt. A more rigorous scientific approach has been followed since 1889, when "modern" scientists started to focus their efforts on what can be defined as the early bone tissue engineering (1). In the wide framework of reconstructive orthopedics, a primary role is played by critical-sized bone defects, which are a large disruption, either a fracture or a hole, typically resulting from severe injuries or traumas, that cannot spontaneously heal because of their size and site (2-4). Both functional and aesthetical reasons make oral and maxillo-facial restorations critical operations: indeed, bone loss due to trauma, infection, or tumor and congenital deformity still remain heavy challenges for surgeons (5, 6).

Hence, the need of adequate bone substitutes for the remodeling of native bone tissue is evident and covers a wide spectrum of proposed solutions, belonging to academia, clinics and industry (7-9).

Key words: bone, cell growth, oral surgery, scaffold, tissue engineering

Mailing address: Prof. Francesco Carinci, Department of Morphology, Surgery and Experimental Medicine, University of Ferrara, Via Luigi Borsari 46, 44100 Ferrara, Italy
e-mail: crc@unife.it
Tel.: +39 0532 455874
Fax: +39 0532 455876

0393-974X (2015)

The current clinical gold standard for treatment of critical sized and non-union bone defects still remain distraction osteogenesis and autograft bone: in particular, autografts are commonly considered the best option to restore defects in oral surgery (10, 11). Although advantageous for immunocompatibility and their self-evident capability to strongly support osteogenesis, osteoinduction and osteoconduction, autografts nevertheless carry a wide spectrum of risks (general anesthesia, second surgical field, infections, fractures, pain, etc.). In addition, there is quite a high percentage of failure (more than 20%); moreover, high costs increase the related to time of surgery (12). Furthermore, larger defects cannot be corrected by harvesting bone from the patient donor site, at least without morbidity in the second surgical field. These major drawbacks have led to the necessity of new methods for bone tissue regeneration (13-15) and today surgeons can choose from substitutes that can be divided into 3 main categories: i) allografts, *i.e.* bone segments taken from cadavers and duly deantigenized sterilized; ii) xenografts, *i.e.* bone segments taken from animal bones, duly processed and sterilized; and iii) synthetic scaffolds and biomaterials.

Allografts derived from cadavers bone have been an accepted alternative, but concerns related to disease transmission, immunologic rejection risks and very high sample variability are progressively leading to other alternatives, when these are available (16). The current focus and major research trends, thus, are on xenografts *vs* synthetic devices (4): naturally-derived materials provide structures extremely similar to living tissues, such as stimulating a specific cellular response, which sometimes supersedes the advantages of synthetic polymers (17, 18). Xenografts may also reduce the stimulation of chronic inflammation or immunological reactions and toxicity, often detected with synthetic polymers and minerals (such as *e.g.* bioglasses and bioceramics) (17-19).

On the other hand, material science, in conjunction with bio- and nano-technologies, can satisfy these requirements by developing novel grafting devices (8, 20, 21). In particular, bioresorbable scaffolds, as key artificial devices widely used in tissue engineering, aim to provide a desirable microenvironment that allows neo-tissue to be generated properly for repairing and replacing damaged tissues or organs (22, 23). Indeed, synthetic polymers can be tuned in terms of composition, rate of degradation, mechanical and chemical properties (17, 19). As a fundamental premise in tissue engineering, polymeric scaffold should provide: (a) host tissue-like mechanical support for promoting neo-tissue ingrowth and functioning (24); (b) adequate porosity and permeability for nutrient delivery and metabolite removal (25); and (c) controllable degradation rate of scaffolding matrix to allow proper substitution with natural functional new tissues (26). Significant progress in tissue engineering could yield more favorable outcomes than the current range of approaches used to repair bone defects (3, 10, 27).

For all these reasons, the goal of our approach was to combine the biocompatibility and tissue integration of natural materials with the possibility to tune mechanical and physical properties typical of synthetic ones: composite grafts best mimic the real nature of healthy human bone, being rigid and elastic, compact but porous, dense but viable to cells and vessels. A newly developed bone substitute, named SmartBone® (briefly SB), was designed following a new concept of bottom-up composite approach, starting from bovine bone-derived mineral matrix, reinforced with bioresorbable aliphatic polymers and RGD-containing collagen fragments as cell nutrients (28, 29).

The bovine-derived matrix is mineral and mainly made of calcium hydroxyapatite (HA, $Ca_5(PO_4)_3(OH)$) that presents a chemical structure and a morphology resembling human bone (30, 31). However, its physical properties have a rigid but not elastic structure, which makes it too fragile. In addition, sterilization processes destroy its natural porous structure, widening it further than natural limits, and does not consent either easy graft manufacturing or cell adhesion. For these reasons bovine structure was reinforced with the addition of an elastic component in terms of polymer coating, thus losing the fragility and reducing porosity to resemble healthy human bones (32). Finally, the addition of RGD-containing collagen fragments, increases the cell viability and hydrophilicity of the scaffold with consequent higher cell attachment, thus enhancing biocompatibility and osteointegration (7, 29, 32). The scaffold produced was firstly characterized in terms of chemistry, microstructure and physical

properties. Then material biocompatibility and suitability as cell growth matrix were studied *in vitro* with SAOS-2 and MG-63 cells. Animal implantation studies, on New Zealand white rabbits (33), and advanced biocompatibility tests were performed according to ISO10993 specifications. Lastly, human studies were performed on critical-sized maxillary and mandibular bone defects to verify SB suitability as scaffold for bone tissue engineering.

MATERIALS AND METHODS

Materials and scaffold preparation

The bovine-derived cancellous bone was sourced as previously described (28), being certified for human use and of BSE/TSE free origin. The choice of polymers was suggested by their potential applicability within the pharmaceutical and biomedical industry and the necessity to obtain scaffolds with suitable mechanical properties. A commercially available copolymer of poly(L-lactic acid) and poly(ε-caprolactone), PLCL, already used in medical applications, was chosen (Purac Biomaterials, Gorinchem, The Netherlands). RGD-containing collagen fragments were also chosen to improve cell viability, hydrophilicity of the matrix and biocompatibility in general, and were sourced in their pharmaceutical grade formulation (Merck, Darmstadt, Germany). All materials were used as received. SB grafts were then obtained by the reinforcement of bovine bone derived matrix with the mixture of PLCL and (Merck, Darmstadt, Germany) through a proprietary process.Validated ethylene oxide sterilization (at BioSter SpA, Bergamo, Italy) was applied after final double layer packing.

Environmental scanning electron microscopy (ESEM) analysis

Environmental scanning electron microscopy analysis and energy dispersive analysis (EDS) were performed on unseeded samples at 10 kV with Evo 50 EP Instrumentation (Zeiss, Jena, Germany) before cell seeding. Each sample was first analyzed on the side surfaces and then halved with a sharp scalpel and the two inner exposed surfaces were finally analyzed (34). Then, at the end of the cell culture studies, scaffolds were fixed with 2.5% (v/v) glutaraldehyde solution in 0.1 M sodium cacodylate buffer for 1 h at 4°C, washed with sodium cacodylate buffer, and then dehydrated at room temperature in a gradient ethanol series up to 100%. The samples were kept in 100% ethanol and then analyzed, again, both on external surfaces and internal ones (35).

Porosity evaluation

Micro computer-assisted tomographic (μ-CT) scan were performed on SB cubic blocks to investigate internal porosity and to numerically evaluate the geometric characteristics of the average SB, *i.e.* free volume and surface to volume ratio (*s/v*). Scan were performed on 10 samples, sized about 8x8x8 mm^3 (*i.e.* ≈ 0.5cc) for analytic reasons, using a VTomEx-s tomograph (Phoenix|x-ray, a GE company, Germany) (34).

Mechanical testing

Uniaxial test was performed using a MTS 858 MiniBionix (Eden Praire, MN, USA) testing machine equipped with a 10 kN calibrated load cell, compressing the specimen between two parallel plates at a constant speed of 1 mm/min: displacement of the upper plate and force were acquired at 10 Hz frequency (28).

Cell culture

The human osteosarcoma cell line SAOS-2 was obtained from the American Type Culture Collection (HTB85, ATCC, Rockville, MD, USA). Following the method used by Pertici et al. (35), cells were cultured in Dulbecco's Modified Eagles Medium DMEM (Sigma-Aldrich, Germany) modified medium with L-glutamine, HEPES (Cambrex Bio Science Baltimore, Baltimore, USA), supplemented with 15% fetal bovine serum, 2% sodium pyruvate, 1% antibiotics, and 0.1 μM puromycin (Invitrogen, Carlsbad, CA, USA). The cells were cultured at 37°C with 5% CO_2, routinely trypsinized after confluence, counted, and seeded. From many cell lines that exhibited osteoblastic features, SAOS-2 cells were selected because they exhibited the most mature osteoblastic phenotype among different osteoblast-like cell lines (36, 37). SB samples were then seeded (6 x 10^4 cells each sample) with SAOS-2 cells by micro seeding technique and incubated at 37°C and 5% CO_2. Cells, at the same concentration, were also seeded on standard polystyrene cell culture plates as control group (CTRL). At different time points, on days 1, 4, 7, 12, 18, 25 and 32, cellular metabolic activity was assessed using an Alamar Blue™ assay (AbD Serotec, UK) where absorbance was measured by spectrophotometry (Genius Plus, Tecan, Italy) at 570 nm.

Histological studies on in vitro cultured samples

At day 25, samples were removed from culture dishes and dipped quickly into liquid nitrogen, then placed in histological common carriers and embedded in paraffin (Paraplast®, 56°C fusion point; SPI supplies, West Chester, PA, USA) following standard histological embedding techniques. Samples were then cut with a microtome, into 3-μm slices, which were placed on microscope slides (SuperFrost®; Menzel-Gläser, Braunschweig, Germany), and stained with hematoxylin and eosin (H&E).

ISO10993 studies

The complete biocompatibility and biological evaluation of SB scaffolds was performed under ISO-10993 standards, particularly addressing: cytotoxicity (with cell culture method); sensitization (applying Guinea pig maximization test); intracutaneous reactivity (on New Zealand rabbits), systemic toxicity test (on lab. mice), implantation (on New Zealand rabbits, with explanations at 4 and 8 weeks post grafting); genotoxicity.

Clinical study

All clinical investigations were carried out after having received specific ethics committee approval (made available to the editor) and under strict observance of the Declaration of Helsinki.

A female patient, 55 years old, good initial health condition underwent surgical intervention, in January 2012, on two different sites, for bone volume recovery for implantation purposes. Specifically: A) surgical site 45-46 was suffering from bone atrophy and was treated with SB 10x10x10 mm blocks, manually sized to fit defect to achieve thickness transverse recovery; B) a post-extractive bone gap was present in site 23, filled with shaped-to-size 7x7x7mm bone block, while the bone loss in neighboring area 24-25 was cross-increased with 10x10x10 mm SB blocks, duly shaped to match bone profile, and SB microchips (1-2mm) to maintain final volume. Surgical follow-up was monitored via intraoral x-ray imaging at month 2; after 4 months, a CT scan was performed to check bone regeneration, and histological sampling was then performed during site preparation for implantation. Further follow-up included controls at months 12 and 24. A final control was carried out by X-ray out after 3 years from SB grafting to prove the healthy and solid structure of newly formed bone.

The second patient was a female, aged 52 years, treated in area 24 for a large bone loss due to fracture: the patient underwent bone reconstruction with SB granules (1 - 2 mm) in January 2012, underwent implant surgery after 5 months and was followed-up at months 8 and 24 with intraoral X-ray.

Bone block regenerative surgery always requires the use of membranes to cover grafts and hence provide separation from soft tissues, mainly to avoid fibroblast proliferation and competition in the graft and to finally maintain tissue separation during the early healing stage. Here, the composite intimate nature of SB called for the strict avoidance of enzymatic-processed membranes, specifically to avoid the eventual activation of residual enzymes by degradation products of the polymers used. Clinical investigations were, hence, performed with regenerated collagen membranes (Resodont Forte, Resorba GmbH, Germany).

Statistical analysis

Experimental data were analyzed using Analysis of Variance (ANOVA); statistical significance was set to P value < 0.05; results are presented as mean ± SD (19).

RESULTS

ESEM analysis and porosity

Native bovine-derived bone scaffold was analyzed from a microstructural point of view using SEM (Fig. 1A): pores were well distributed along the sample but they were extremely larger in respect to those present in healthy human iliac crest bones, (Fig. 1B). Comparing the SB scaffold (Fig. 1C) with human cortical iliac crest bone sample (Fig. 1B) a strong resemblance between them is clearly visible: both exhibited a similar porous structure confirming the obtained SB scaffold as suitable for bone tissue engineering.

MicroCT scans supported these statements as they confirmed a strong resemblance with human cortical bone in terms of open and interconnected mid-sized porosity, with an average 27% (±2%) of free volume and an average s/v of 4.46mm^{-1} (*i.e.* a free surface of about 2.3mm^2 out of a volume of 512mm^3, as also previously shown (34).

Analyzing the inner surface of the sample (Fig. 1D), the porous structure and the two parts were more evidently visible: mineral and polymer were easily distinguishable; furthermore EDS spectrum of zone 1 in Fig. 1E was characterized by strong element signals of C and O confirming the presence of the polymeric film, while in the cavity (zone 2) the presence of Ca and P showed the mineral part of the sample corresponding to HA (Fig. 1F). In addition, Fig. 1G evidenced the inner surface of SB scaffold after being cut, exhibiting great evidence of mineral matrix coated with polymeric film. Structural differences between mineral fraction and polymer were highlighted by backscatter image (Fig. 1G, left). The corresponding EDS analysis, performed (yellow line) from the surface to the inner part of the sample, is presented in Fig. 1H: it highlighted C (red) as polymer presence on the surface of the scaffold while the increasing presence of Ca (blue) moving to its inner part highlighted the mineral nature of the matrix.

Compressive properties

Compressive tests were performed to evaluate the

Table I. *Compressive properties of the SB and native bone scaffold scaffolds: maximum stress, compressive modulus and fracture strength.*

Mechanical properties	SB scaffold	Native bone scaffold
Maximum compression stress [MPa]	28	7.5
Compressive modulus [GPa]	0.5	0.07
Fracture strength [MPa]	14	7

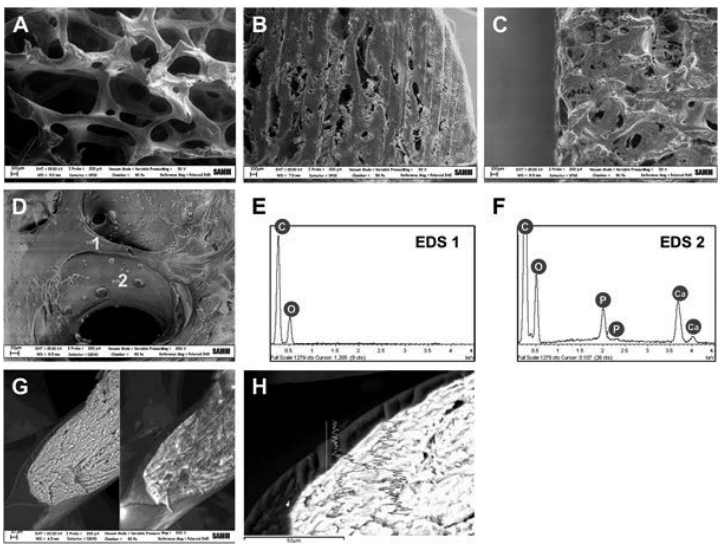

Fig. 1. A, B, C) *ESEM images at the same magnitude (bar scales = 100 µm) of bovine scaffold (A), healthy human iliac crest bone sample (B) and polymer coated SB scaffold (C).* ***D, E, F)*** *SB scaffold ESEM image (scale bar = 20 µm) and corresponding EDS spectra. Spot 1 is characterized only by the strong signals of C and O, typical of the presence of polymer film and spot 2 characterized by the presence of Ca and P, confirming the mineral nature of the matrix.* ***G, H)*** *SB scaffold ESEM image (scale bar = 10 µm) and corresponding EDS spectrum (scale bar = 50 µm). It evidences the outer polymer film while signal of Ca indicates the inner mineral part of the sample.*

mechanical properties of the SB scaffold in terms of maximum stress, compressive modulus and fracture strength: stress was obtained dividing the recorded force by the initial cross-section area while strain was calculated as the recorded displacement divided by the initial height of the specimen. Moreover, the effect of polymer coating and reinforcement was investigated comparing SB with native bone scaffold. As shown in Fig. 2 and Table I, the maximum stress, compressive modulus and fracture strength of the modified SB scaffolds were higher than those of the native bone scaffold. In detail, compression of SB scaffolds evidenced a maximum stress resistance (28 MPa av.) and a Young's modulus (0.5 GPa av.). From a mechanical point of view, SB scaffolds were found to be more rigid and comparable with human bone ones, underlining the necessity of the previously described reinforcement process (Table I).

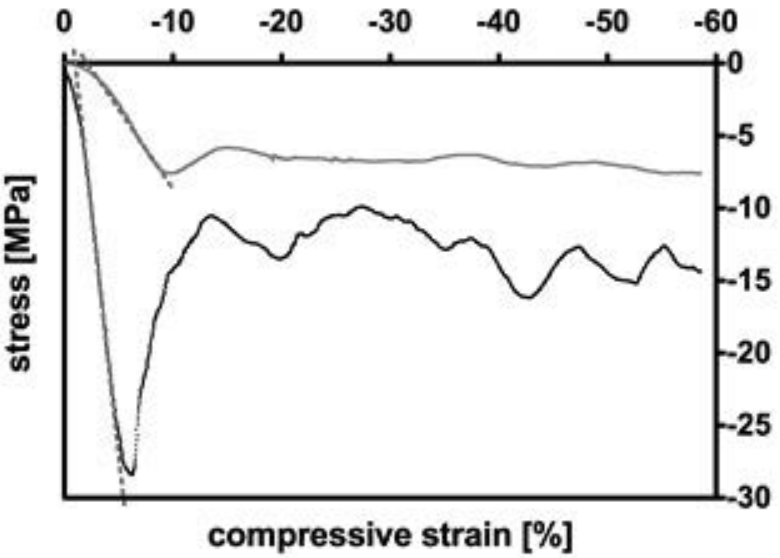

Fig. 2. *Compressive stress vs. strain plot of native bone (grey and upper line) and SB (black and lower line) scaffolds.*

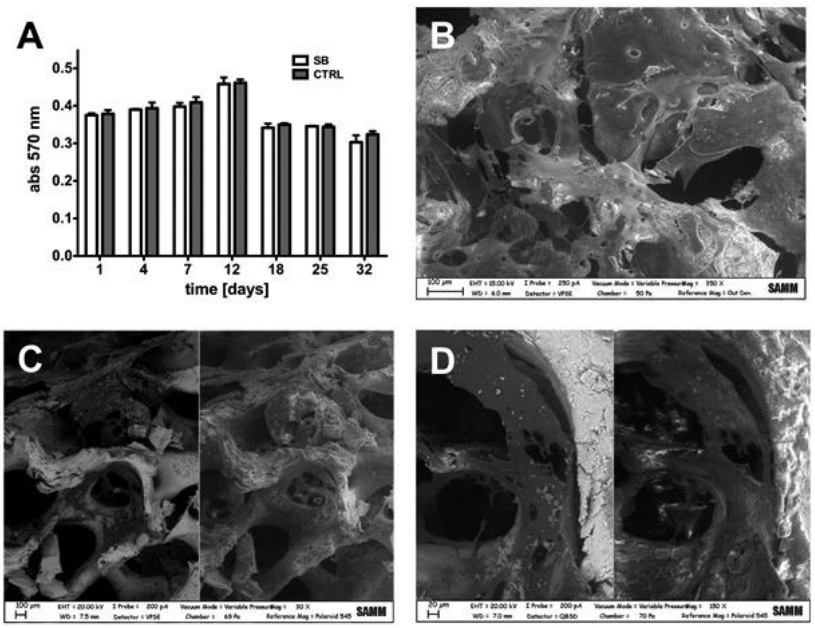

Fig. 3. A) *Alamar BlueTM staining indicating comparable values and profiles between P-BS and control (CTRL) groups at each time point (p > 0.005) for SAOS-2 cells seeded within SB scaffolds;* ***B, C, D)*** *ESEM images at different magnification of SAOS-2 cells seeded on SB scaffold after 25 days.* ***E)*** *Alamar BlueTM staining indicating comparable values and profiles between SB and control (CTRL) groups at each time point (p > 0.005) for MG-63 cells seeded within SB scaffolds;* ***F)*** *ESEM image of MG-63 cells seeded within SB scaffold after 8 days. Bar scales: 100 µm (B), 100 µm (C), 20 µm (D) and 100 µm (F).*

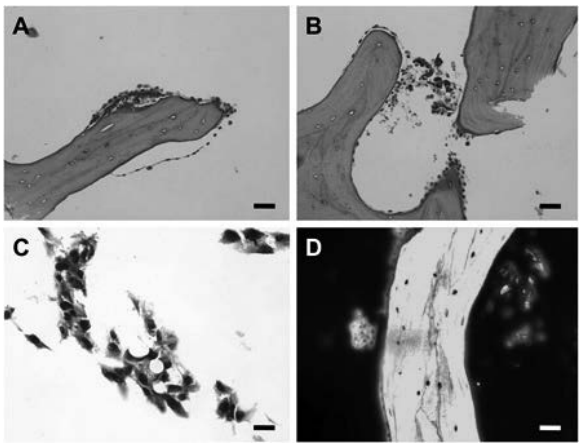

Fig. 4. *Histologic images of SAOS-2 after 25 days culture within SB scaffold. (A, B, D) H&E staining shows cell morphology and spread inside SB scaffold; the massive cell proliferation onto the thin polysaccharide and copolymer coating, thus confirmed its importance as enhancer of cell adhesion; (C) H&E staining shows cell morphology and spread inside SB scaffold. Bar scales: 200 µm (A), 200 µm (B), 50 µm (C) and 100 µm (D).*

In vitro cell morphology and viability

SAOS-2 cell morphology, within SB scaffolds, was firstly visualized by ESEM images (Fig. 3B, C, D). Fig. 3B is a representative image of 25 days within SB scaffolds, showing adherence of cells to their surface. In particular, the cells covered homogeneously the polymeric coating surface. ESEM results indicate that SAOS-2 cells were confluent and displayed an elongated spindle shape and therefore capable of proliferating and adhering to SB scaffold. At higher magnification (Fig. 3B, C) it was easily visible that cells adhered to the polymeric coating, highlighting the importance of polymer coating to allow cell growth.

The ability of cells to adhere and proliferate was quantitatively assessed by measuring their cellular metabolic activity with Alamar Blue™ assay, as reported in Fig. 3A. Alamar Blue™ assay was used as an indicator of cell proliferation, provided the metabolic activity per cell can be assumed to be relatively constant and not strongly dependent on cell morphology or substrate type. Cell numbers (Fig. 3A) were found to be similar for all the investigated time between SAOS-2 seeded within SB scaffold and control group (CTRL) cultured in classic polystyrene cell culture plates. Similar results were collected also with MG-63 cell line (Fig. 3, E and F).

Fig. 4 shows H&E-stained histological sections of SB scaffolds harvested at 25 days post cell seeding. In Fig. 4A, it can be seen that cells were able to colonize, adhere and spread within the SB scaffold. The H&E stain demonstrated homogeneity in cell distribution and adhesion along the scaffold. The seeded cells proliferated in a multilayer fashion, and there were more cells observed at the surface than in the interior of the scaffold as seen in Fig. 4B. Massive cell proliferation onto the thin polysaccharide and copolymer PLCL coating confirmed its importance as enhancer of cell adhesion. The morphology of cells was well visible, as reported in Fig. 4D, and was in complete accordance with ESEM images (Fig. 3). The use of fluorescent SAOS-2 cells (Fig. 4D) helped us to observe and confirm the colonization of the scaffold, underlining the importance of the reinforcement present in SB scaffolds.

ISO10993 studies

Standard compulsory ISO-10993 investigations on biocompatibility were carried out, under GLP conditions, specifically: Intracutaneous Reactivity Test, Systemic Toxicity Test and Delayed Hypersensitivity Test were performed, all resulting completely negative, thus confirming SB full biocompatibility.

Clinical studies

The implanted SB material used in this study, bone blocks, proved to be elastic and sufficiently robust to be precisely handled and cut to the necessary shape and dimensions in order to best fit (Fig. 5B) the specific patient bone defect (Fig. 5A). The material is not friable, hence it was easily fixed to the receiving bone, previously duly microcanalized, with osteosynthesis screws (Fig. 5B), and the radiography after 2 months post-implantation underlined the good placement of the graft (Fig. 5C): tight and stable contact with the receiving site is essential for bone regeneration. Regenerated ridges healed uneventfully. No post-operative complications

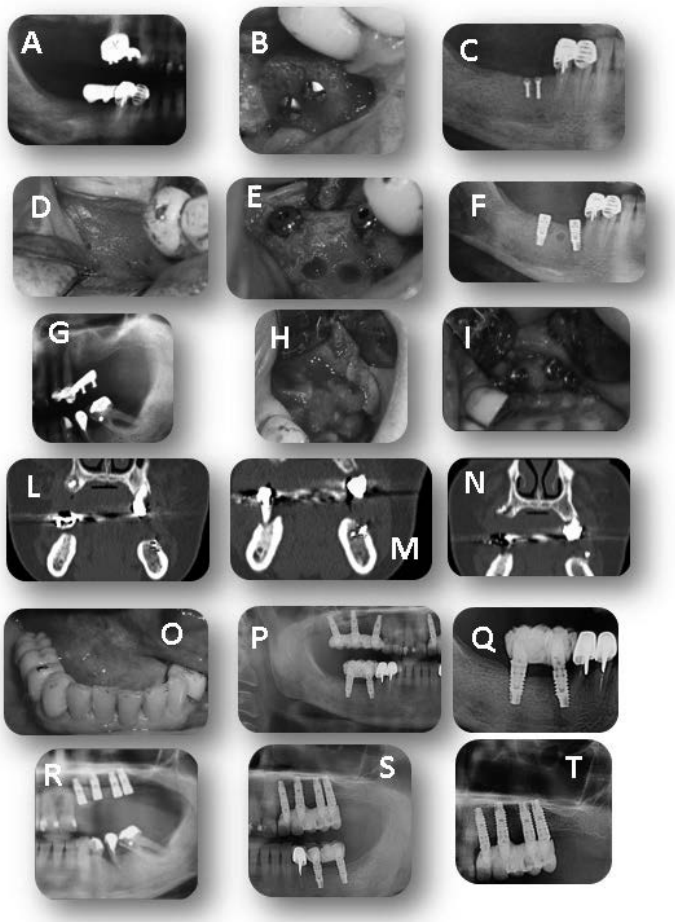

Fig. 5. *Clinical SB studies:* ***A)*** *specific patient bone defect;* ***B)*** *SB bone blocks precisely handled and cut to the necessary shape and dimensions and hence fixed with osteosynthesis miniscrews;* ***C)*** *radiography after 2 months post implantation underlined the good placement of the graft;* ***D)*** *4 months after grafting no evidences of serious adverse local side effects, like inflammation, pain or dehiscence, was observed;* ***E)*** *4 months after grafting implanted material could not be identified in the regenerated sites, being already integrated and capable of sustaining safe implants placement;* ***F)*** *robustness of integration after only 4 months allowed sustaining deep histological sampling;* ***G)*** *same patient, upper surgical site;* ***H)*** *miniscrew fixing and tight mechanical stabilization of SB graft onto bone defect space; I) implant positioning already after 4 months, on a sufficiently strong and dense SB graft; L,M,N) examples of Hounsfield analysis performed on CT scan slices taken 4 months after grafting, showing a well-integrated SB graft, with a good structure and density around mini-screws (i.e. exactly where the graft was) of about an average of 500 HU; O,P,Q) follow-up after 1, 2 and 3 years for lower site and R,S,T) for upper one, respectively, proved robust evidences of good bone formation, x-ray analysis gave high density signals and bone morphology and structure 3 years after grafts appeared comparable with healthy contralateral ones.*

were present after the ridge augmentation and at the time of the implantation surgery. Four months after grafting no evidence of serious adverse effects, such as inflammation, pain or dehiscence, was observed (Fig. 5D), and no implanted material was identified in the regenerated sites (Fig. 5E). From radiography (Fig. 5F) it was visible that newly-formed bone was similar to the surrounding tissue. Moreover, new bone, thanks to its mechanical properties, consented to fix screws for dental implants, as is visible from the radiography (Fig. 5F), and to sustain histological sampling. Similar performances and results were recorded on the upper surgical site (Fig. 5G), where SB mechanical performances allowed both

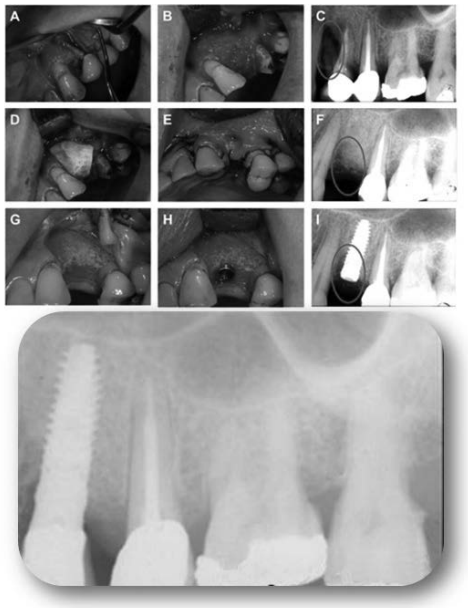

Fig. 6. *A, B, C) Bone defect visions and radiography (C) where bone defect is visible by black color; (D, E) granulated SB grafting; (F) radiography that underlines new bone formation 4 months after grafting procedure; (G) 4 months after implantation good tissue regeneration and osteointegration are observable; (H) screws for dental implants fixation to the new bone 4 months after scaffold implantation; (I) radiography after 8 months underlines bone regrowth and the possibility to fix on it screws for dental implants; (L) radiographic follow-up after 2 years proved robust evidences of good bone formation.*

miniscrew fixing and tight mechanical stabilization onto bone defect space (Fig. 5H). Regenerated bone was tough already after 4 months, sufficiently strong and dense as to easily withstand positioning of implants, as needed (Fig. 5I).

Hounsfield analysis performed on CT scan slices taken 4 months after grafting showed a well integrated SB graft, with a good structure and density: bone density around mini-screws (*i.e.* exactly where the graft was) had an average of 500 HU (Fig. 5. L,M,N). Indeed, the new bone allowed fixing the screw for dental implant (Fig. 5. E-I), and controls showed their good placement and alignment with patient teeth. Follow-up after 1, 2 and 3 years (Fig. 5 O,P,Q for the lower site and Fig 5 R,S,T for the upper site, respectively) proved concrete evidence of good bone formation. X-rays showed high density signals and bone morphology and structure 3 years after grafts which appeared comparable with the healthy contralateral ones. No more graft distinction was possible, nor were discontinuity lines evident from 4 months post-surgery.

Similar results were found also for the second patient: the bone defect was studied and granulated SB were mixed with patient blood and tailor-made to obtain the desired shape once *in situ*. The bone defect was visible (Fig. 6A-B) also in the radiography (Fig. 6C). SB was successfully grafted and covered with a commercial resorbable collage membrane (Fig. 6D). Good osteointegration together with new bone formation were already visible 4 months later (see radiography in Fig. 6F). The new bone allowed fixing screw for dental implant (Fig. 6G, H) and the radiography after 8 months (Fig. 6I) showed their good placement and alignment with the patient's teeth. Similarly to above, follow-up after 2 years proved concrete evidence of good bone formation (Fig. 6L).

In summary, these cases demonstrated successful bone reconstruction with polymer-coated mineral scaffolds implanted *in situ*. Furthermore, the histological analysis of the biopsies demonstrated an intense new formation of bone around the SB graft (bone with empty gaps) and several lines of new bone growth, thus highlighting a good osteoconduction of the biomaterial (Fig. 7 A-F presents slides from case A, lower site, as indicative examples). SB was progressively substituted by new young bone. Inside the new bone matrix, the purple lines (growth-lines) indicated a good osteoinduction (Fig. 7 C-D). This phenomenon is also evidenced by osteoblast presence on the outer surface of the newly formed bone where young woven bone is present. The slices clearly show osteocytes within the gaps and a hint of bone lamellae, therefore the bone is in a maturing process. Indeed, at high magnifications, the images show newly formed, not yet mature bone, as shown by the presence of much larger nuclei within the gaps (not yet quiescent osteoblasts) and a woven bone around them (Fig. 7 E-F).

DISCUSSION

Porosity and pore size of biomaterials play a key role in osteointegration and new bone formation (38). Relatively larger pores favor direct

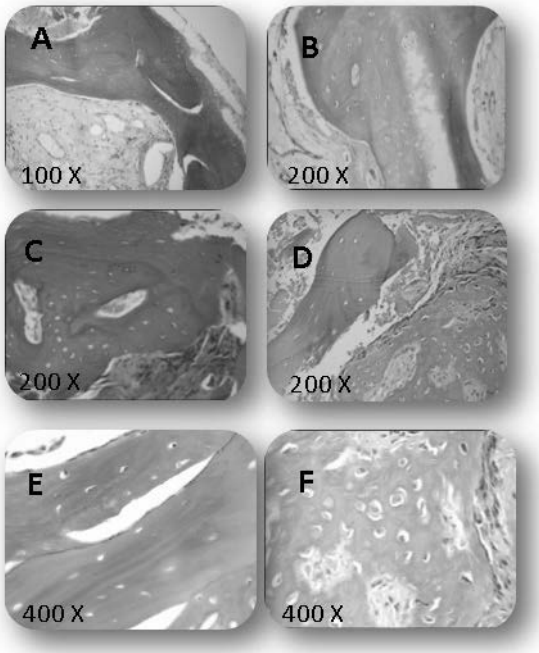

Fig. 7. *Exemplificative histological slides from case A, lower site, respectively: A) showing an intense new formation of bone around the SB graft and several lines of new bone growth; B) indicating SB is progressively substituted by new young bone; C-D) they shown a good osteoinduction; high magnifications images showing newly formed, not yet mature bone, as evidenced by the presence of much larger nuclei within the gaps (not yet quiescent osteoblasts) and a woven bone around them.*

osteogenesis, since they allow vascularization and high oxygenation, while smaller ones result in osteochondral ossification. There is, however, an upper limit in porosity and pore size set by constraints associated with mechanical properties. An increase in the void volume results in a reduction in mechanical strength of the scaffold, which can be critical for regeneration in load-bearing bones. The differences of bone tissues in morphological (pore size and porosity) and mechanical properties set challenges for fabricating biomaterial scaffolds that can meet the requirements set by the specific site of application. Therefore, following these statements, polymer reinforcement seems to be essential to reduce the pore sizes with the aim of mimicking healthy human bone microstructure, presented in Fig. 1B. As known, macroscopic properties of matter are a direct reflection of microscopic ones: here, the presence of the biopolymer film also plays a key role in the mechanical resistance of this new composite bone substitute. As shown in Fig. 2 and Table I, the composition of a mineral matrix, representing a rigid component, with polymers, being the elastic element, allow to obtain a much better performing device which shows resistance and elasticity comparable to target human ones. Moreover, the high and well-known biocompatibility of chosen polymers, together with the thin layering, allows SB to be a cell-supporting scaffold, where cells find the appropriate substrate to adhere to and grow, as shown in Fig. 3. Biocompatibility was among the key criteria to be precisely followed when choosing SB components: all constituents were chosen among those already available on the market of human-approved substances and devices. This choice can be considered a type of "design and development philosophy", where the innovation lies in making a composite out of safe and known components: safety, not only as a result of biocompatibility, is an unavoidable target, which was definitely proven during all mandatory ISO studies. Having straightforwardly and successfully passed all characterization and safety tests.

The key element is RGD-sequence containing proteins, physically entrapped into the thin polymeric layer: proteins that contain the Arg-Gly-Asp (*a.k.a.* RGD) attachment site, together with the integrins that serve as receptors for them, constitute a major recognition system for cell adhesion. Such peptides promote cell adhesion when insolubilized onto a surface (29). Histological analyses performed during human studies confirmed that SB supports the ingrowth of osteoblasts, which then spread and colonize it, hence generating new bone. Furthermore, the ensemble made by SB and the patient's receiving system is osteo-inductive: SB not only serves as a scaffold for currently existing osteoblasts but will also trigger the formation of new osteoblasts, also deriving from stromal stem cells, promoting faster integration of the graft.

In this study, a composite scaffold made of natural mineral matrix (calcium hydroxyapatite) and synthetic polymer coating (PLCL) with the addition of RGD-containing collagen fragments was *ex novo* developed

and investigated. The purpose behind coating mineral scaffold with PLCL and RGD-containing collagen fragments came from the necessity to have higher mechanical properties together with suitable microstructure and to improve hydrophilicity for good cell adhesion and viability, to gain high osteoinductive properties. The fabricated scaffold exhibited a regular microstructure similar to healthy iliac bones (*i.e.* the most commonly harvested autograft) and high ability to allow cell growth using human standard cell lines. The results achieved showed high cell adhesion to the scaffolds and viability values similar to the control groups. SB grafting in human cases was validated in maxillary and mandibular bone defects: in all the specimens presented in this study newly formed bone was visible. No inflammation or foreign body reactions were observed, and these findings confirm animal studies evidence and support the good biocompatibility of SB composite material. The new bone was observed in close contact with the implanted material and neither gaps nor fibrous tissues were observed at the interface. The cellular response to SB graft can be described as a progressive neoformation of healthy bone, which occurs alongside the reabsorbtion of the graft, where both osteoconductive and osteoinductive processes are involved between grafts and receiver bone sites. In summary, all this evidence demonstrates the good suitability of SB grafts for bone regeneration.

ACKNOWLEDGEMENTS

The authors would like to thank the Biocompatibility and Cell Culture (BioCell-Lab, Politecnico di Milano, Italy) Laboratory staff for their cooperation and Dr Mariotti (Università degli Studi di Milano, Italy) for having provided SAOS-2 cell line.

We wish to draw the attention of the Editor to the following facts which may be considered as potential conflicts of interest and to significant financial contributions to this work: two authors, Gianni Pertici and Giuseppe Perale, are affiliated to the Company manufacturing the bone substitute object of this study (as evident from the authors and affiliations).

REFERENCES

1. Senn on the Healing of Aseptic Bone Cavities by Implantation of Antiseptic Decalcified Bone. Ann Surg 1889; 10(5):352-368.
2. Cordonnier T, Sohier J, Rosset P, Layrolle P. Biomimetic materials for bone tissue engineering – state of the art and future trends. Advanced Engineering Materials 2011; 13:135-150.
3. Chen FM, An Y, Zhang R, Zhang M. New insights into and novel applications of release technology for periodontal reconstructive therapies. J Control Release 2011; 149(2):92-110.
4. Mourino V, Boccaccini AR. Bone tissue engineering therapeutics: controlled drug delivery in three-dimensional scaffolds. J R Soc Interface 2010; 7(43):209-227.
5. Zhou M, Peng X, Mao C, Xu F, Hu M, Yu GY. Primate mandibular reconstruction with prefabricated, vascularized tissue-engineered bone flaps and recombinant human bone morphogenetic protein-2 implanted in situ. Biomaterials 2010; 31(18):4935-4943.
6. Gronthos S. Reconstruction of human mandible by tissue engineering. Lancet 2004; 364(9436):735-736.
7. Isikli C, Hasirci V, Hasirci N. Development of porous chitosan-gelatin/hydroxyapatite composite scaffolds for hard tissue-engineering applications. J Tissue Eng Regen Med 2012; 6(2):135-143.
8. Langer R. Perspectives and challenges in tissue engineering and regenerative medicine. Adv Mater 2009; 21(32-33):3235-3236.
9. Hutmacher DW, Schantz JT, Lam CX, Tan KC, Lim TC. State of the art and future directions of scaffold-based bone engineering from a biomaterials perspective. J Tissue Eng Regen Med 2007; 1(4):245-260.
10. Zou D, Zhang Z, He J, et al. Repairing critical-sized calvarial defects with BMSCs modified by a constitutively active form of hypoxia-inducible factor-1alpha and a phosphate cement scaffold. Biomaterials 2011; 32(36):9707-9718.
11. Di Stefano DA, Artese L, Iezzi G, Piattelli A, Pagnutti S, Piccirilli M, Perrotti V. Alveolar ridge regeneration with equine spongy bone: a clinical, histological, and immunohistochemical case series. Clin Implant Dent Relat Res 2009; 11(2):90-100.
12. Gitelis S, Saiz P. What's new in orthopaedic surgery. J Am Coll Surg 2002; 194(6):788-791.

13. Chen M, Le DQ, Baatrup A, Nygaard JV, Hein S, Bjerre L, Kassem M, Zou X, Bunger C. Self-assembled composite matrix in a hierarchical 3-D scaffold for bone tissue engineering. Acta Biomater 2011; 7(5):2244-2255.
14. Duailibi SE, Duailibi MT, Zhang W, Asrican R, Vacanti JP, Yelick PC. Bioengineered dental tissues grown in the rat jaw. J Dent Res 2008; 87(8):745-750.
15. Manferdini C, Guarino V, Zini N, et al. Mineralization behavior with mesenchymal stromal cells in a biomimetic hyaluronic acid-based scaffold. Biomaterials 2010; 31(14):3986-3996.
16. Nolan P, Templeton P, Mollan RA, Wilson DJ. Osteoinductive potential of human demineralised bone and a bioceramic in abdominal musculature of the rat. J Anat 1991; 174:97-102.
17. Shoichet MS. Polymer Scaffolds for Biomaterials Applications. Macromolecules 2010; 43:581–591.
18. Costa-Pinto AR, Reis RL, Neves NM. Scaffolds based bone tissue engineering: the role of chitosan. Tissue Eng Part B Rev 2011; 17(5):331-347.
19. Perale G, Rossi F, Sundstrom E, Bacchiega S, Masi M, Forloni G, Veglianese P. Hydrogels in spinal cord injury repair strategies. ACS Chem Neurosci 2011; 2(7):336-345.
20. Stevens MM. Biomaterials for bone tissue engineering. Materialstoday 2008; 11:18-25.
21. Brey DM, Chung C, Hankenson KD, Garino JP, Burdick JA. Identification of osteoconductive and biodegradable polymers from a combinatorial polymer library. J Biomed Mater Res A 2010; 93(2):807-816.
22. Kim J, Sharma A, Runge B, et al. Osteoblast growth and bone-healing response to three-dimensional poly(epsilon-caprolactone fumarate) scaffolds. J Tissue Eng Regen Med 2012; 6(5):404-413.
23. Arafat MT, Lam CX, Ekaputra AK, Wong SY, Li X, Gibson I. Biomimetic composite coating on rapid prototyped scaffolds for bone tissue engineering. Acta Biomater 2011; 7(2):809-820.
24. Sturm S, Zhou S, Mai YW, Li Q. On stiffness of scaffolds for bone tissue engineering-a numerical study. J Biomech 2010; 43(9):1738-1744.
25. Karande TS, Ong JL, Agrawal CM. Diffusion in musculoskeletal tissue engineering scaffolds: design issues related to porosity, permeability, architecture, and nutrient mixing. Ann Biomed Eng 2004; 32(12):1728-1743.
26. Rose FR, Oreffo RO. Bone tissue engineering: hope vs hype. Biochem Biophys Res Commun 2002; 292(1):1-7.
27. Lin CY, Chang YH, Kao CY, Lu CH, Sung LY, Yen TC, Lin KJ, Hu YC. Augmented healing of critical-size calvarial defects by baculovirus-engineered MSCs that persistently express growth factors. Biomaterials 2012; 33(14):3682-3692.
28. Pertici G, Müller M, Perale G. Bioresorbable bioactive matrix for bone regeneration. Tissue Engineering Part A 2010; 16.
29. Duong LT, Rodan GA. Integrin-mediated signaling in the regulation of osteoclast adhesion and activation. Front Biosci 1998; 3:d757-768.
30. He J, Genetos DC, Leach JK. Osteogenesis and trophic factor secretion are influenced by the composition of hydroxyapatite/poly(lactide-co-glycolide) composite scaffolds. Tissue Eng Part A 2010; 16(1):127-137.
31. Kane RJ, Roeder RK. Effects of hydroxyapatite reinforcement on the architecture and mechanical properties of freeze-dried collagen scaffolds. J Mech Behav Biomed Mater 2012; 7:41-49.
32. Jeong SI, Lee AY, Lee YM, Shin H. Electrospun gelatin/poly(L-lactide-co-epsilon-caprolactone) nanofibers for mechanically functional tissue-engineering scaffolds. J Biomater Sci Polym Ed 2008; 19(3):339-357.
33. Moimas L, Biasotto M, Di Lenarda R, Olivo A, Schmid C. Rabbit pilot study on the resorbability of three-dimensional bioactive glass fibre scaffolds. Acta Biomater 2006; 2(2):191-199.
34. Pertici G, Rossi F, Casalini T, Perale G. Composite polymer-coated mineral grafts for bone regeneration: material characterisation and model study. Annals of Oral & Maxillofacial Surgery 2014; 2.
35. Pertici G, Maccagnan S, Mueller M, Rossi F, Daniele F, Tunesi M, Perale G. Porous biodegradable microtubes-based scaffolds for tissue engineering, part I: production and preliminary in vitro evaluation. J Appl Biomater Biomech 2008; 6(3):186-192.
36. Saino E, Grandi S, Quartarone E, et al. In vitro calcified matrix deposition by human osteoblasts onto a zinc-containing bioactive glass. Eur Cell

Mater 2011; 21:59-72; discussion 72.
37. Leidi M, Dellera F, Mariotti M, Banfi G, Crapanzano C, Albisetti W, Maier JA. Nitric oxide mediates low magnesium inhibition of osteoblast-like cell proliferation. J Nutr Biochem 2012; 23(10):1224-1229.
38. Karageorgiou V, Kaplan D. Porosity of 3D biomaterial scaffolds and osteogenesis. Biomaterials 2005; 26(27):5474-5491.